ELSEVIER

Chemical Engineering Journal 132 (2007) 125–135

Chemical Engineering Journal

www.elsevier.com/locate/cej

Temperature and pressure fields due to collapsing bubble under ultrasound

Ki Young Kim, Ki-Taek Byun, Ho-Young Kwak *

Mechanical Engineering Department, Chung-Ang University, Seoul 156-756, Republic of Korea

Received 22 September 2006; received in revised form 18 January 2007; accepted 20 January 2007

Abstract

Temperature and pressure fields generated by the collapsing bubble of microsize in liquid under ultrasound are estimated by a set of solutions of the Navier–Stokes equations for the gas inside bubble with considering heat transfer through the bubble wall. The calculation results for the peak temperature and pressure were compared to the observed ones from a sonoluminescing bubble which can be levitated in a spherical cell under ultrasound frequency range of 10–40 kHz. The calculation results are in good agreement with observed ones. However, the Rayleigh–Plesset equation with polytropic relation, a conventional method yields considerably underestimated values in temperature and overestimated ones in pressure. The bubble dynamics model presented in this study may be used as a tool for the design of sonochemical reactor where the peak temperature and pressure and the pressure field due to the bubble collape are important parameters.

Keywords: Temperature and presusre fields; Acoustic cavitation; Bubble dynamics; Ultrasound

1. Introduction

It is well known that high-power ultrasound at a frequency range of 20 kHz enhances the rate or various chemical reactions [1,2] through the generation and subsequent growth and collapse of microsize bubbles which provide hot spot region of high temperature and pressure in the liquid layer adjacent to bubble [3]. In fact, degradation of organic compounds in aqueous solutions [4,5] and synthesis of new materials with better yields and/or shorter times through the acoustic cavitation [6,7] at the frequency of 20 kHz were reported. At the multibubble sonoluminescence (MBSL) condition achieved in cylindrical cell at an ultrasound frequency of 20 kHz and a power input of 165 W, methylene blue (MB) was degraded completely [8]. Even uniform coating of CdS particles on TiO_2 nanoparticles was succeeded through a one pot reaction under the MBSL condition [9].

Recently, optimum design for better processing of various chemical reactors [10,11] and scale-up sonochemical reactor for industrial applications [12] were studied. As a design tool, usually the Rayleigh–Plesset equation for the bubble wall motion and the polytropic relation for the gas behavior inside the bubble under ultrasound have been employed. The cavitation intensities represented by the peak temperature and pressure achieved at the collapse of microbubble, which are very important parameters for the sonochemical reactor design can be predicted hardly by the polytropic relation. In fact, the polytropic relation conjunction with the Rayleigh–Plesset equation provides considerable overestimation of the peak pressure and underestimation of the peak temperature for a sonoluminescing gas bubble [13] in sulfuric acid solutions [14,15]. Further the polytropic approximation fails to account for the thermal damping effect due to finite heat transfer through the bubble wall during bubble evolution because $P_b\,dV$ is perfect differential [16]. Another serious question on the use of the polytropic approximation is that it is very hard to tell whether the gas inside the bubble under ultrasound behaves isothermally or adiabatically [17,18].

A rather homogeneous bubble size distribution with an average diameter of 10 μm was obtained in a sonochemical reactor at a driving frequency of 20 kHz with an input power of 179 W by using the phase-Doppler technique [19]. This observation suggests that individual behavior of the bubbles with this size range should be studied for the design of sonochemical reactors. However, for the bubble whose radius is less than 10 μm, relaxation behavior of bubble with respect to the driving ultrasound was obtained [20–22], which should be taken into account in the study of bubble dynamics.

* Corresponding author. Tel.: +82 2 820 5278; fax: +82 2 826 7464.
E-mail address: kwakhy@cau.ac.kr (H.-Y. Kwak).

1385-8947/$ – see front matter © 2007 Elsevier B.V. All rights reserved.
doi:10.1016/j.cej.2007.01.037

Nomenclature

C_B	sound speed at the bubble wall
$C_{p,b}$	heat capacity of gas at constant pressure
$C_{v,b}$	heat capacity of gas at constant volume
e	internal energy per mass
f_d	frequency of ultrasound
k_g	conductivity of gas
k_l	conductivity of liquid
n	polytropic index
P_A	driving ultrasound amplitude
P_b	pressure inside bubble
P_{b0}	pressure at the bubble center
P_s	driving ultrasound pressure
Pe	Péclet number
q_r	heat flux inside bubble
r	radius from the bubble center
R_b	radius of bubble
$\dot{R}_b$	bubble wall velocity
R_0	equilibrium radius of bubble
t	time
T_b	temperature of gas inside bubble
T_{bl}	temperature at the bubble–liquid interface
T_{b0}	temperature at the bubble center
u_g	gas velocity inside bubble
U_b	bubble wall velocity

Greek letters

α	thermal diffusivity of liquid
γ	specific heat ratio of gas
Γ	polytropic index
δ	thermal boundary layer thickness
δ_p	momentum boundary layer thickness
μ	dynamic viscosity of liquid
ρ_g	gas density inside bubble
ρ_r	radially dependent gas density
ρ_0	gas density at the bubble center
ρ_∞	density of liquid medium
σ	interfacial tension
ω	angular frequency of ultrasound

Subscripts

b	bubble
0	center
∞	ambient liquid medium

Since a levitation technique of a single bubble in a cylindrical cell by ultrasound has been developed [23], various exotic phenomena related to the single sonoluminescing bubble in a spherical or cylindrical cell have been unveiled [24,25]. The calculation results were compared to the observed ones from the single sonoluminescing bubble in various spherical cells under ultrasound frequency range of 10–45 kHz. It is noted that the equilibrium size of the bubble levitation spherical cell is determined by the cell size, ultrasound frequency, gas species inside the bubble and host liquid.

In this study, the behavior of an individual bubble with microsize under ultrasound was studied by using a set of solutions of the Navier–Stokes equations for the gas inside bubble by considering heat transfer with a parabolic temperature distribution for the liquid layer adjacent to the bubble wall. The lagging behavior of microsize bubble with respect to the applied ultrasound was also considered. The calculation results of bubble radius–time curve, and the peak temperature and pressure were compared to the observed ones and the calculated ones by the polytropic approximation and direct numerical simulation and a discussion on the obtained results was made.

2. Bubble dynamics

2.1. Hydrodynamic solutions for the gas inside bubble

The hydrodynamics related to the bubble behavior in liquid under ultrasound involves solving the Navier–Stokes equations for the gas inside bubble and the liquid adjacent to the bubble wall. The mass conservation for the gas inside the bubble with spherical symmetry is given as

$$\frac{\partial \rho_g}{\partial t} + \frac{1}{r^2}\frac{\partial}{\partial r}(\rho_g u_g r^2) = 0 \tag{1}$$

With decomposition of the gas density into center and radial-dependent parts such as [18]:

$$\rho_g = \rho_0(t) + \rho_r(r,t) \tag{2}$$

the continuity equation becomes

$$\left[\frac{\partial \rho_0}{\partial t} + \rho_0 \frac{1}{r^2}\frac{\partial}{\partial r}(u_g r^2)\right] + \left[\frac{\partial \rho_r}{\partial t} + \frac{1}{r^2}\frac{\partial}{\partial r}(\rho_r u_g r^2)\right] = 0 \tag{3}$$

Since the rate of change of the density of a material particle can be represented by the rate of volume expansion of the particle in the limit $V \to 0$ [26], or

$$\nabla \cdot \vec{u}_g(r) = \lim_{V\to 0}\left(\frac{\dot{V}}{V}\right) = \frac{3\dot{R}_b}{R_b} \tag{4}$$

the radial-dependent velocity profile inside the bubble may be written as

$$u_g = \frac{3\dot{R}_b}{R_b} r \tag{5}$$

With this velocity profile, a set of solutions for the mass conservation equation may be obtained. These are

$$\rho_0 R_b^3 = \text{const.} \tag{6}$$

and

$$\rho_r = \frac{ar^2}{R_b^5} \tag{7}$$

The constant a is related to the gas mass inside a bubble by $a/m = 5(1 - N_{BC})/4\pi$ with $N_{BC} = (P_{b0}R_b^3/T_{b0})/(P'_\infty R_0^3/T_\infty)$, where $P'_\infty = P_\infty + 2\sigma/R_0$.

The momentum conservation for the gas with spherical symmetry is given as

$$\frac{\partial}{\partial t}(\rho_g u_g) + \frac{1}{r^2}\frac{\partial}{\partial r}(\rho_g u_g^2 r^2) + \frac{\partial P_b}{\partial r} = 0 \tag{8}$$

The gas pressure inside the bubble P_b can be obtained from the momentum equation with the density and velocity profiles given in Eqs. (2) and (5), respectively [27]. Or

$$P_b = P_{b0} - \frac{1}{2}\left(\rho_0 + \frac{1}{2}\rho_r\right)\frac{\ddot{R}_b}{R_b}r^2 \tag{9}$$

The linear velocity profile showing the spatial inhomogeneities inside the bubble is a crucial ansatz for the homologous motion of a spherical object, which is encountered in another energy focusing mechanism of gravitational collapse [28]. The quadratic pressure profile given in Eq. (9), was verified recently by comparisons with direct numerical simulations [29]. It is also noted the uniform temperature that distribution is achieved when the bubble oscillation period is much shorter than the characteristic time of the heat diffusion, $t_d = R_b^2/\alpha_g$ [17] and the uniform pressure inside the bubble can be achieved if the bubble wall acceleration is less than 10^{12} m/s^2 [30].

Assuming that the internal energy for the gas inside a bubble is a function of gas temperature only as $de = C_{v,b}\,dT_b$, the energy equation for the gas inside the bubble may be written as

$$\rho_g C_{v,b}\frac{DT_b}{Dt} = -\frac{P_b}{r^2}\frac{d}{dr}(r^2 u_g) - \frac{1}{r^2}\frac{d}{dr}(r^2 q_r) \tag{10a}$$

The viscous dissipation term in the internal energy equation also vanishes because of the linear velocity profile. Since the solutions given in Eqs. (2), (5) and (9) also satisfy the kinetic energy equation, only the internal energy equation given in Eq. (10a) needs to be solved. Wu and Robert [31] and Moss et al. [32] tried to solve numerically the total energy equation without the heat transfer term along with the mass and momentum equations given in Eqs. (1) and (8), respectively. However, their calculation without considering the heat transfer inside the bubble and in the liquid layer at the bubble wall considerably overestimated the gas temperature in the bubble [32]. On the other hand, Prosperetti et al. solved the internal energy equation combined with the mass and momentum equation numerically to consider heat transport inside the bubble. However, heat transfer through the liquid layer, which is very important to obtain the temperature at the bubble wall was not considered in their study. While Yasui [33] considered only heat transfer through the liquid layer with a simple assumption for the boundary layer. It is also noted that it is very hard to obtain a temperature distribution from the energy equation, Eq. (10a) because $C_{v,b}$ is a nonlinear function of temperature when the vibration motion of molecules become active and dissociation and ionization occur at high temperature, which should be considered for investigating the radiation mechanism of sonoluminescence [34].

Using the definition of enthalpy, the internal energy equation for the gas can be also written as

$$\rho_g C_{p,b}\frac{DT_b}{Dt} = \frac{DP_b}{Dt} - \frac{1}{r^2}\frac{\partial}{\partial r}(r^2 q_r) \tag{10b}$$

Eliminating D/Dt $(=\partial/\partial t + u_g\partial/\partial r)T_b$ from Eqs. (10a) and (10b), one can obtained the following heat transport equation for the gas pressure inside bubble [18,27]:

$$\frac{DP_b}{Dt} = -\frac{\gamma P_b}{r^2}\frac{\partial}{\partial r}(r^2 u_g) - \frac{\gamma - 1}{r^2}\frac{\partial}{\partial r}(r^2 q_r) \tag{11}$$

With help of the solutions given in Eqs. (2), (5) and (9), Eq. (11) becomes

$$\frac{\gamma - 1}{r^2}\frac{\partial}{\partial r}(r^2 q_r) = -\left[\frac{dP_{b0}}{dt} + 3\gamma P_{b0}\frac{\dot{R}_b}{R_b}\right] + \frac{1}{2}\left(\rho_0 + \frac{1}{2}\rho_r\right) \times \left[(3\gamma - 1)\frac{\dot{R}_b\ddot{R}_b}{R_b^2} + \frac{\dddot{R}_b}{R_b}\right]r^2 \tag{12}$$

Since the temperature rise due to the bubble wall acceleration is a transient phenomenon occurred during few nanoseconds, the above equation may be decomposed into

$$\frac{\gamma - 1}{r^2}\frac{\partial}{\partial r}(r^2 q_0) = -\left[\frac{dP_{b0}}{dt} + 3\gamma P_{b0}\frac{\dot{R}_b}{R_b}\right] \tag{13a}$$

and

$$\frac{\gamma - 1}{r^2}\frac{\partial}{\partial r}[r^2(q_r - q_0)] = \frac{1}{2}\left(\rho_0 + \frac{1}{2}\rho_r\right)\left[(3\gamma - 1)\frac{\dot{R}_b\ddot{R}_b}{R_b^2} + \frac{\dddot{R}_b}{R_b}\right]r^2 \tag{13b}$$

A temperature profile without the bubble wall acceleration can be obtained by solving Eq. (13a) with the Fourier law. That is [18]:

$$T_b(r) = \frac{B}{A}\left[-1 + \sqrt{\left(1 + \frac{A}{B}T_{b0}\right)^2 - 2\eta\frac{A}{B}(T_{bl} - T_\infty)\left(\frac{r}{R_b}\right)^2}\right] \tag{14}$$

where A and B are the coefficients in the temperature-dependent gas conductivity having a form such as $k_g = AT + B$ and $\eta = (R_b/\delta)(k_l/B)$. For xenon $A = 1.031 \times 10^{-5}$ J/ms K^2 and $B = 3.916 \times 10^{-3}$ J/ms K and for argon $A = 2.685 \times 10^{-5}$ J/ms K^2 and $B = 1.347 \times 10^{-3}$ J/ms K were used [35]. The temperature distribution given in Eq. (14) is valid until the characteristics time of the bubble evolution is on the order of the relaxation time for the vibrational motion of the molecules [18] and/or is much less than the relaxation time of the translational motion of the molecules [36].

Abrupt temperature rise and subsequent rapid quenching due to the bubble wall acceleration and the increase and decrease in the acceleration may be treated in another time scale [37], different from the bubble motion. A solution of Eq. (13b) with no temperature gradient at the bubble center is given as

$$T_b'(r) = -\frac{1}{40(\gamma - 1)k_g'}\left(\rho_0 + \frac{5}{21}\rho_r\right) \times \left[(3\gamma - 2)\frac{\dot{R}_b\ddot{R}_b}{R_b^2} + \frac{\dddot{R}_b}{R_b}\right]r^4 + C(t) \tag{15}$$

The coefficient C may be determined from a boundary condition $k'_g\,dT_b/dr = k_l\,dT_l/dr$ at the wall where T_l is the temperature distribution in the thermal boundary layer with a different thickness of δ'. That is,

$$C = \frac{1}{20(\gamma-1)}\left[(3\gamma-2)\dot{R}_b\ddot{R}_bR_b + \dddot{R}_bR_b^2\right] \times \left[\frac{\delta'}{k_l}\left(\rho_0 + \frac{5}{14}\rho_{r=R_b}\right) + \frac{R_b}{2k'_g}\left(\rho_0 + \frac{5}{21}\rho_{r=R_b}\right)\right] \quad (16)$$

The gas conductivity at ultra-high temperatures may be obtained from the collision integrals [38]. The value of δ' may be chosen so that proper bouncing motion results after the collapse and is about 0.1 μm. The final solution of the heat transport equation can be represented by the superposition of the temperature distributions caused by the uniform pressure and by the radial pressure variation induced by the rapid change of the bubble wall acceleration, as can be seen in Eq. (9); that is,

$$T(r) = T_b(r) + T'_b(r) \quad (17)$$

2.2. Governing equations from the Navier–Stokes equations for the liquid adjacent to the bubble wall

The mass and momentum equation for the liquid outside the bubble wall provides the well-known equation of motion for the bubble wall [39], which is valid until the bubble wall velocity does not exceed the sound speed of the liquid. That is,

$$R_b\left(1-\frac{U_b}{C_B}\right)\frac{dU_b}{dt} + \frac{3}{2}U_b^2\left(1-\frac{U_b}{3C_B}\right) = \frac{1}{\rho_\infty}\left(1+\frac{U_b}{C_B}+\frac{R_b}{C_B}\frac{d}{dt}\right)\left[P_B - P_s\left(t+\frac{R_b}{C_B}\right) - P_\infty\right] \quad (18)$$

The liquid pressure on the external side of the bubble wall P_B is related to the pressure inside the bubble wall P_b by $P_B = P_b - 2\sigma/R_b - 4\mu U_b/R_b$. The pressure of the driving sound field P_s may be represented by a sinusoidal function such as $P_s = -P_A \sin\omega t$ where $\omega = 2\pi f_d$.

The temperature distribution in the liquid layer adjacent to the bubble wall, which is important to determine the heat transfer through the bubble wall is assumed to be quadratic [40], such as

$$\frac{T-T_\infty}{T_{bl}-T_\infty} = (1-\xi)^2 \quad (19)$$

where $\xi = (r-R_b)/\delta$. Such second-order curve satisfies the following boundary conditions.

$$T(R_b,t) = T_{bl}, \qquad T(R_b+\delta,t) = T_\infty \quad \text{and} \quad \left(\frac{\partial T}{\partial r}\right)_{r=R_b+\delta} = 0 \quad (20)$$

The mass and energy equation for the liquid layer adjacent to the bubble wall with the temperature distribution given in Eq. (14) provides a time-dependent first-order equation for the thermal boundary layer thickness [18]. It is given by

$$\left[1+\frac{\delta}{R_b}+\frac{3}{10}\left(\frac{\delta}{R_b}\right)^2\right]\frac{d\delta}{dt} = \frac{6\alpha}{\delta} - \left[2\frac{\delta}{R_b}+\frac{1}{2}\left(\frac{\delta}{R_b}\right)^2\right]\frac{dR_b}{dt} - \delta\left[1+\frac{1}{2}\frac{\delta}{R_b}+\frac{1}{10}\left(\frac{\delta}{R_b}\right)^2\right]\frac{1}{T_{bl}-T_\infty}\frac{dT_{bl}}{dt} \quad (21)$$

Such integral method, which can be classified as one member of weighted residual methods, is particularly well suited to the problem where the time-dependent variable $T_{bl}(t)$ on the bubble wall is time-dependent. With thin boundary layer approximation, $\delta/R_b \ll 1$ and with fixed value of the wall superheat, $T_{bl} - T_\infty$, Eq. (21) provides a well known thermal boundary layer thickness of order of $(\alpha t)^{1/2}$ and asymptotic limit of bubble growth due to heat diffusion [41]. In fact, the heat transfer associated with the oscillatory motion of the bubble is negligibly small. The above equation determines the heat flow rate through the bubble wall. Instantaneous bubble radius, bubble wall velocity and acceleration and the thermal boundary thickness obtained from Eqs. (18) and (21) provide density, velocity, pressure and temperature profiles for the gas inside the bubble without any further assumptions. No adjusted parameter is needed for calculation. The gas temperature and pressure at the bubble center can be obtained from the ideal gas law $\rho_0 R_b^3 = \text{const.}$, one of the solutions for the continuity equation given in Eq. (1).

The momentum boundary layer thickness δ_p, associated with the pressure gradient may be obtained by integrating the momentum equation for the liquid layer adjacent to the bubble wall with assumption of an incompressible fluid. An equation to obtain the thickness of the momentum boundary layer, which was used to predict the barodiffusion, a mass flow due to the pressure difference between the gas pressure inside the bubble and ambient pressure [42], is given by

$$\frac{P_b - P_\infty}{\rho_\infty \dot{R}_b^2} = -\frac{\alpha_p}{1+\alpha_p}\left[\frac{3\left(\alpha_p + (4/3)\alpha_p^2 + (1/2)\alpha_p^3\right)}{1+3\alpha_p+3\alpha_p^2+\alpha_p^3} + \frac{R_b\ddot{R}_b}{\dot{R}_b^2}\right] \quad (22)$$

where $\alpha_p = \delta_p/R_b$. The bubble dynamics model presented above permits to predict correctly the bubble radius–time curve and the bubble wall velocity at the collapse point [20].

2.3. Prosperetti et al.'s formulation

Assuming that the internal pressure is uniform and the gas behaves like ideal gas, Prosperetti et al. [16] obtained the following equation by using Eqs. (1) and (10):

$$\nabla\cdot u_g = \frac{1}{\gamma P_g}\left[(\gamma-1)\nabla\cdot(k_g\nabla T_b) - \frac{dP_g}{dt}\right] \quad (23)$$

The above equation is just Eq. (11) for the case of uniform pressure. An integration of Eq. (23) over the volume of the bubble leads to the velocity profile inside the bubble such as

$$u_g(r,t) = \frac{1}{\gamma P_g}\left[(\gamma-1)k_g\frac{\partial T_b}{\partial r} - \frac{1}{3}r\frac{dP_g}{dt}\right] \quad (24)$$

The time-dependent gas pressure inside the bubble can be obtained from the above equation by evaluating it at $r = R_b$. That is,

$$\frac{dP_b}{dt} = \frac{3}{R_b}\left[(\gamma-1)k_g\left(\frac{\partial T_b}{\partial r}\right)_{r=R_b} - \gamma P_b U_b\right] \quad (25)$$

The internal energy given in Eq. (10b) for the case of uniform pressure can be rewritten with ideal gas law, $P_b = \rho_g R T_b$ where R is gas constant, such as

$$\frac{\gamma}{\gamma-1}\frac{P_b}{T_b}\left(\frac{\partial T_b}{\partial t} + u_g\frac{\partial T_b}{\partial r}\right) - \frac{dP_b}{dt} = \frac{1}{r^2}\frac{\partial}{\partial r}\left(r^2 k_g\frac{\partial T_b}{\partial r}\right) \quad (26)$$

Eqs. (24)–(26) replace the mass, momentum and energy conservation, respectively. The distributions for the gas velocity and temperature inside the bubble can be obtained by solving Eqs. (24)–(26) simultaneously at a given time with proper numerical method [43]. In their study, the temperature distribution in the liquid adjacent to the bubble wall is assumed to be negligible so that the interface temperature is maintained to be equal to ambient one. Considerable computation time, however, is needed to obtain reasonable results with this formulation when the characteristic time of bubble evolution is nanosecond range or below.

The temperature distribution for the gas inside bubble with the boundary condition which Prosperetti et al. [16] have chosen can also be obtained by solving Eq. (13a) with help of the set of solutions of the Navier–Stokes equation for the gas inside the bubble. That is,

$$T_b(r) = \frac{B}{A}\left[-1 + \sqrt{\left(\frac{A}{B}T_{b0}+1\right)^2 - \left\{\left(\frac{A}{B}T_{b0}+1\right)^2 - \left(\frac{A}{B}T_\infty+1\right)^2\right\}\left(\frac{r}{R_b}\right)^2}\right] \quad (27)$$

As is well known, the above temperature distribution indicates the case of maximum heat transfer through the bubble wall regardless of the thermal properties of liquid.

2.4. Other approximations

For the calculation of the gas pressure inside bubble Hilgenfeldt et al. [44] employed the following van der Waals equation with polytropic exponent of Γ:

$$P_b = \left(P_\infty + \frac{2\sigma}{R_b}\right)\left(\frac{R_0^3 - h^3}{R_b^3 - h^3}\right)^\Gamma \quad (28)$$

where $h = R_0/8.5$ is the hard-core van der Waals radius for air and the polytropic index Γ is taken to be unity, which is called by "process equation" by theirs. However, the polytropic index value of unity has not been used to obtain the gas pressure inside the bubble usually [45]. Certainly, Eq. (28) which assumed the isothermal and uniform behavior of the gas inside bubble is not adequate to estimate the gas temperature inside the bubble. For calculating the temperature, they employ the following relation to obtain the polytropic exponent, n which depends on Péclet number:

$$n = 1 + (\gamma-1)\exp\left[-\frac{B}{Pe^A}\right] \quad (29)$$

where γ is the specific heat ratio and the numerical values of A and B are 5.8 and 0.6, respectively. The time-dependent, instantaneous Péclet number for the oscillating bubble is given by

$$Pe = |\dot{R}_b|\frac{R_b}{\alpha_g} \quad (30)$$

Unphysical picture of their model with variable polytropic index exists around the bubble collapse: the polytropic index becomes unity at $\dot{R}_b = 0$ at the collapse point where adiabatic process is dominant. It is better to use the polytropic index of n, which is related to the thermal diffusivity of the gas and liquid and driving sound frequency [46] to obtain gas temperature by using the following equation:

$$\frac{T_b}{T_\infty} = \left(\frac{R_0^3 - h^3}{R_b^3 - h^3}\right)^{n-1} \quad (31)$$

For air bubble under ultrasound frequency of 16–1000 kHz range, the polytropic index needed to calculated the temperature is about 1.3. Note that the uniform temperature obtained from Eq. (31) is valid when thermal equilibrium prevails inside bubble. The assumption of uniform temperature is good one when the characteristic time of bubble evolution is millisecond range [18].

A summary of this section is as follows. A set of solutions for the mass, momentum and energy equations of the gas inside the oscillating bubble under ultrasound are introduced. Also the equations for the bubble motion and the thermal boundary layer thickness, which can be obtained from the mass, momentum and energy equations for the liquid outside the bubble wall are introduced to obtain instantaneous density, pressure and temperature profiles for the bubble. Another methods to obtain these parameters are also presented.

3. A numerical integration of equation for bubble wall motion

Usually, Eq. (18) the Keller–Miksis (KM) equation cannot be integrated numerically, without normalization by appropriate physical variables. The radius is compared to the equilibrium radius R_0, and the velocity and pressure are related to constants, $u_0 = (P_\infty/\rho_\infty)^{1/2}$ and $P_0 = P_\infty$, respectively. The constants for normalizing other physical quantities such as time, dynamic

viscosity and surface tension of liquid were obtained from the condition that the KM equation becomes homogeneous after the normalization procedure [18,27]. They are given as

Time: $t_0 = R_0/u_0$
Thermal conductivity: $k_0 = P_\infty u_0 R_0/T_\infty$
Thermal diffusivity: $\alpha_0 = u_0 R_0$
Dynamic viscosity: $\mu_0 = P_\infty R_0/u_0$
Surface tension: $\sigma_0 = P_\infty R_0$

The governing equation is normalized by the time scale of $t_0 = R_0/u_0$, the characteristic time of the bubble motion. Also the time t and the driving frequency f_d in the sinusoidal term in Eq. (18) may be normalized by t_0 and $1/t_0$, respectively [47,48] so that the nondimensional form of the sinusoidal term becomes $\cos(2\pi ft)$ where $f = f_d t_0$ is the nondimensional frequency. This may be called as single-time scale normalization (STN) method. However, the STN method yields a bubble behavior moving in phase with the driving ultrasound, which might cause an artificial resonance for bubbles with equilibrium radius of microsize [20,21]. The reduction in the nondimensional frequency in the sinusoidal term with STN yields quite different results for bubble motion in numerical evaluation. For example, the expansion ratio calculated by the Rayleigh–Plesset (RP) equation with STN is as much as 17.2 while the observed value is about 9.76 for an air bubble of $R_0 = 5.0\,\mu m$ driven at $f_d = 12.926\,kHz$ and $P_A = 1.33\,atm$ [21]. The bubble radius–time curves obtained by the modified Rayleigh–Plesset (RP) equation [49] or KM equation with consideration of the relaxation time were found to be virtually same except the bouncing behavior [18], which suggests that the relaxational motion of the bubble against the applied ultrasound is very important in the bubble behavior of microsize.

In general, the characteristic frequency of the driving force f_0 differs from the natural frequency of bubble oscillation $1/t_0$. The time t and the driving frequency f_d in the sinusoidal term in Eq. (18) may be normalized by $1/f_0$ and f_0, respectively so that the sinusoidal term remains in the same form as $\cos(2\pi ft)$ but with different nondimensional frequency $f = f_d/f_0$. Because the bubble wall motion described by Eq. (18) is also normalized by t_0 with this normalization method, but the nondimensional time is recovered by $1/f_0$ in the numerical procedure (which may be called as two-time scale normalization (TTN) method), there is a lag time of the bubble motion with respect to the characteristic time of the applied ultrasound f_0, which is defined as [20]:

$$\tau = \frac{1}{f_0} - t_0 \tag{32}$$

The bubble behavior under ultrasound can be described correctly with the concept of such lag time [22], which is due to the combined effect of the surface tension and viscosity of fluid [49].

4. Calcuation results and discussion

The calculated radius–time curve along with observed results by the light scattering method for a xenon bubble with

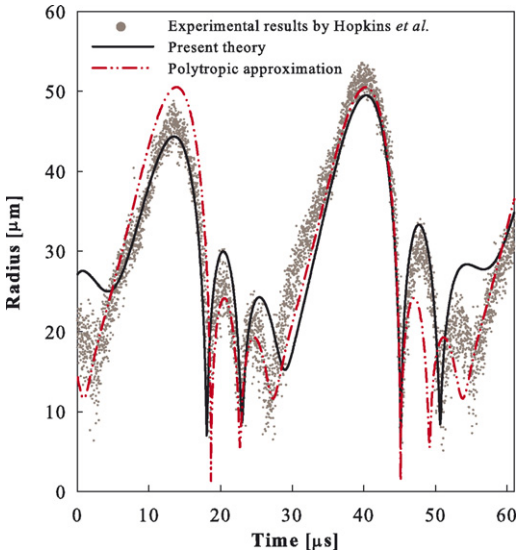

Fig. 1. Theoretical radius–time curve along with observed one by Hopkins et al. [14] for xenon bubble of $R_0 = 15.0\,\mu m$ at $P_A = 1.50\,atm$ and $f_d = 37.8\,kHz$ in sulfuric acid solution. The thermodynamic properties employed for 85% sulfuric acid solution are $\rho = 1800\,kg/m^3$, $C_s = 1470\,m/s$, $\mu = 0.025\,N\,s/m^2$, $\sigma = 0.055\,N/m$, $k_l = 0.40\,W/m\,K$, and $C_{p,l} = 1817\,J/kg\,K$.

$R_0 = 15\,\mu m$, driven by the ultrasonic field with a frequency 37.8 kHz and amplitude of 1.5 atm in aqueous solution of sulfuric acid is shown in Fig. 1. With xenon data for the thermal conductivity, the calculated radius–time curve which mimics the alternating pattern of the observed result shows two different states of bubble motion. On the other hand, the Rayleigh–Plesset equation with polytropic relation, a conventional method [47] used to predict the sonoluminescence phenomena, cannot predict the two states of bubble motion as shown in Fig. 1. It is noted that a stable sonoluminescing bubble was levitated in a spherical, 52 mm diameter (50 cm^3 volume), quartz flask at a ultrasound amplitude of 1.5 atm and frequency of 37.0 kHz, which is a resonance of the flask by Troia et al. [50].

In Fig. 2, the calculated time rate changes of the gas temperature at the bubble center for the bubble shown in Fig. 1 are

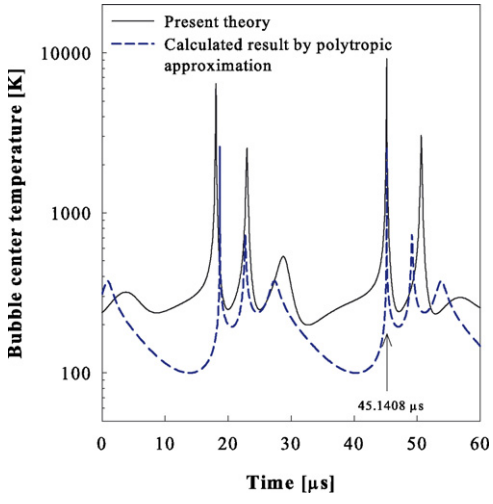

Fig. 2. Calculated bubble center temperatures for the cases shown in Fig. 1.

given. The calculation results by our method revealed that the slow bubble expansion in response to the rarefaction phase of the applied ultrasound undergoes almost isothermally while the subsequent rapid bubble collapse proceeds nearly adiabatically. On the other hand, considerably lower temperature as low as 100 K is achieved at the point of the maximum bubble radius when the bubble evolution was assumed to be proceeded by the polytropic process with $n = 1.3$. Our estimated value of the gas temperature at the collapse point is about 8200 K at the bubble center with the average value of 6000 K, which is close to the observed value of 6000–7000 K by spectrum data fitted to the blackbody radiation [15]. However, the polytropic approximation provides considerable underestimation of the gas temperature of 2300 K at the collapse point.

Because $P_b\,dV$ is a perfect differential and the polytropic relation is a point function so that the gas pressure and the temperature estimated by the polytropic relation does not depend on the process in which the bubble evolves. This is why a "process equation" was proposed to estimate the gas pressure [44]. However, the process equation of $PV = \text{const.}$ which was introduced to estimate the gas pressure cannot account the thermal damping due to finite heat transfer through the bubble wall.

Fig. 3 shows the temperature distribution inside the bubble around the maximum expansion phase (a) and around the collapse one (b). As shown in Fig. 3a an inversion of the temperature distribution occurs before and after the maximum expansion. Before maximum expansion, the temperature at the bubble wall is slightly higher than that at the center so that heat flow from liquid to the bubble occurs. On the other hand, after the maximum expansion point where thermal equilibrium prevails, heat flows out to the liquid, which is drastically different from the results obtained with the polytropic relation. Considerable temperature gradient is built up at the collapse point so that large amount of heat flows into the liquid as shown in Fig. 3b.

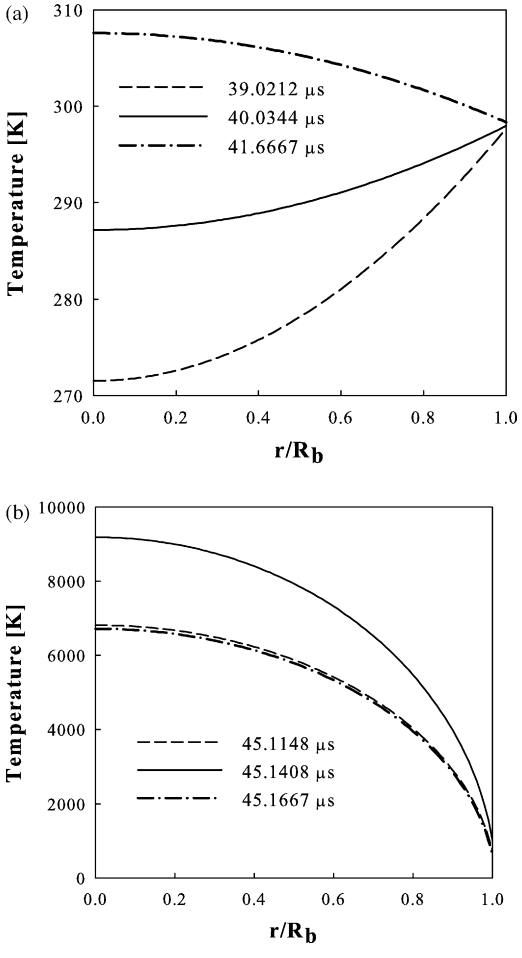

Fig. 3. Temperature distribution (a) near the maximum expansion point and (b) near the collapse point for the bubble shown in Fig. 1.

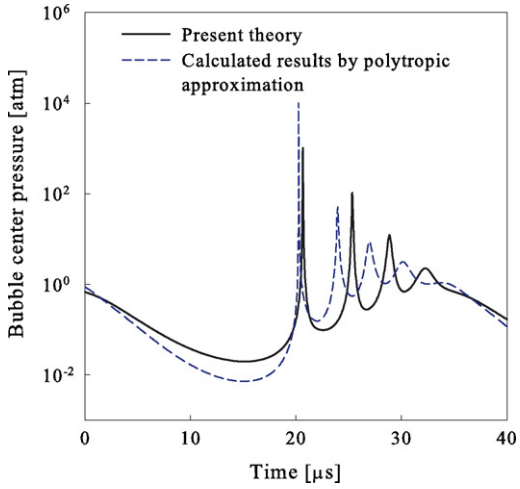

Fig. 4. Calculated gas pressure depending on time for an argon bubble of $R_0 = 13.0\,\mu m$ at $P_A = 1.40$ atm and $f_d = 28.5$ kHz.

Fig. 4 shows the calculated time rate change of the gas pressure for the argon bubble of $R_0 = 13\,\mu m$ at $P_A = 1.4$ atm and $f_d = 28.5$ kHz in sulfuric acid solutions. Our calculated pressure at the collapse point is about 1020 atm, which is close to the observed value of 1090 atm by plasma diagnostics technique [15]. However, considerable overestimation in the gas pressure at the collapse point results with the polytropic relation. As can be seen in Figs. 3 and 4, the calculated time rate change of the gas temperature and pressure inside the bubble by ours are quite different from those obtained by the Rayleigh–Plesset equation with the polytropic relation. Same as the case of the bubbles under ultrasound in sulfuric acid solutions, considerable overestimation in the gas pressure and underestimation in the gas temperature are provided by the polytropic relation for an oscillating bubble in water. The polytropic assumption for the bubble behavior may be a good approximation for small-amplitude case [46].

For a bubble whose equilibrium radius is less than 10 μm, the lagging motion of the bubble with respect to the driving ultrasound should be considered as discussed in previous section. Fig. 5 shows the calculated radius–time curve along with observed one for an air bubble of $R_0 = 8.5\,\mu m$, driven by ultrasound with a frequency of 26.5 kHz and an amplitude of 1.075 atm. Our radius–time curve was calculated with different time scales for the bubble motion t_0 given in Eq. (32) and for the applied ultrasound $1/f_0 = 10^{-6}$ s so that the retarded time of the bubble motion with respect to the driving force τ is about 0.15 μs. Close agreement between our calculated curve and the

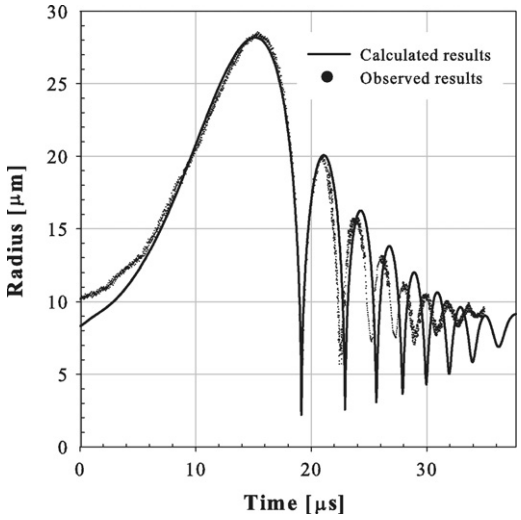

Fig. 5. Theoretical radius–time curve with relaxation time of 0.15 μs along with observed one for air bubble of $R_0 = 8.5$ μm at $P_A = 1.075$ atm and $f_d = 26.5$ kHz in water.

observed one [48] can be seen. However, the curve obtained by the Rayleigh–Plesset equation with a polytropic relation of $PV^{1.4} = \text{const.}$ and without the legging time is quite different from the observed one; the time elapsed from the start to the first bubble collapse is about 16.5 μs compared to the observed value of 19.1 μs and the number of bouncing is 10 rather the observed number of 7 as shown in Fig. 6. Also the magnitude of the maximum bubble radius at the first bounce is significantly less than the observed one.

Fig. 7 shows the calculated bubble radius-time curves along with observed one for an air bubble of $R_0 = 5$ μm under an ultrasound frequency of 12.926 kHz and amplitude of 1.33 atm [21]. As shown in Fig. 7, the curves obtained by Keller–Miksis or modified Rayleigh–Plesset equation with a relaxation time of 0.396 μs mimic correctly the observed behavior of bubble in water. However, the maximum radius calculated without considering the relaxation time is about 1.8 times larger than the

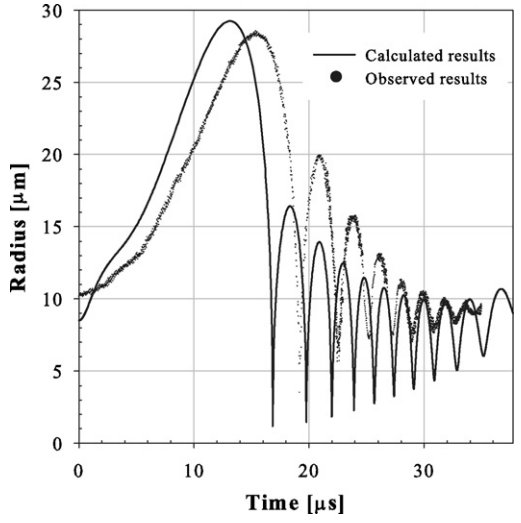

Fig. 6. Calculated radius–time curve obtained from the RP equation with polytropic relation along with observed one for the case shown in this figure.

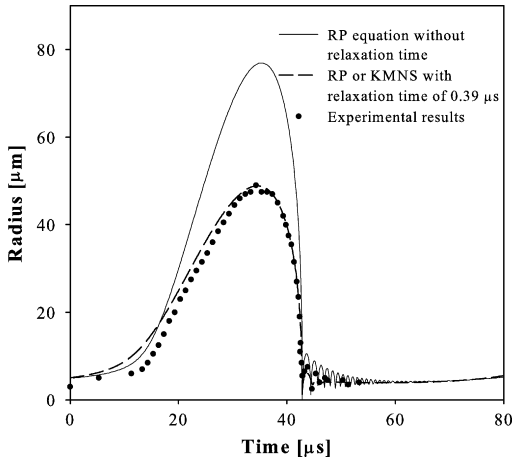

Fig. 7. Radius–time curves from the RP equation without relaxation time (—) and KMNS (- - -) with the relaxation time of 0.39 μs for an air bubble of $R_0 = 5.0$ μm at $P_A = 1.33$ atm and $f_d = 12.926$ kHz in water.

observed one. In consequence of this, the bubble wall velocity at the collapse point, which exceeds 2000 m/s, is much larger than the observed value of 1400 m/s [51]. For reference purpose, snapshot images of the oscillating bubble with accompanying sonoluminescence for the case shown in Fig. 7 are shown in Fig. 8. Clearly can be seen from the image near the collapse point (65 μs), no evaporation of water at the bubble wall where considerable high temperature above the critical temperature of water is expected, occurs.

As shown in Fig. 9, the bubble wall acceleration near the collapse point for the bubble shown in Fig. 7 exceeds 10^{12} m/s^2 so that a thermal spike due to abrupt rise and subsequent decrease in the bubble wall acceleration appears. The thermal spike which lasts only fraction of nanosecond as shown in Fig. 9 generates a light pulse due to Bremsstrahlung [27,30]. In this case, the temperature distribution due to the bubble wall motion after the flash and the corresponding heat flux inside bubble are show in Fig. 10. The maximum temperature at the bubble center is about 28,000 K and the maximum heat flux at the bubble wall is as much as 35 TW/m^2. Of course, these values become lower at a high frequency of 30 kHz operation as shown in Figs. 11 and 12. On the other hand the maximum temperature estimated by the polytropic relation with $n = 1.3$ is about 6700 K even though the bubble radius at the collapse point is as small as 0.16 μm.

Fig. 11 shows the bubble radius–time curves obtained from the direct numerical simulation (DNS) by Storey [52], polytropic assumption, and our method, for a radius of 4.5 μm bubble forced with a 1.3 atm pressure amplitude at 32.8 kHz. The calculation results by DNS and our theory with $\tau = 0$, produced similar radial oscillations including the boundary motion after the collapse. On the other hand, polytropic assumption yields quantitatively incorrect results because the thermal damping due to the finite heat transfer across the bubble wall cannot be taken into account.

Fig. 12a shows the time-dependent temperature and pressure at the bubble wall around the collapse point and Fig. 12b shows spatial temperature and pressure distributions in the liquid layer adjacent to the bubble wall at the collapse point. As can be seen

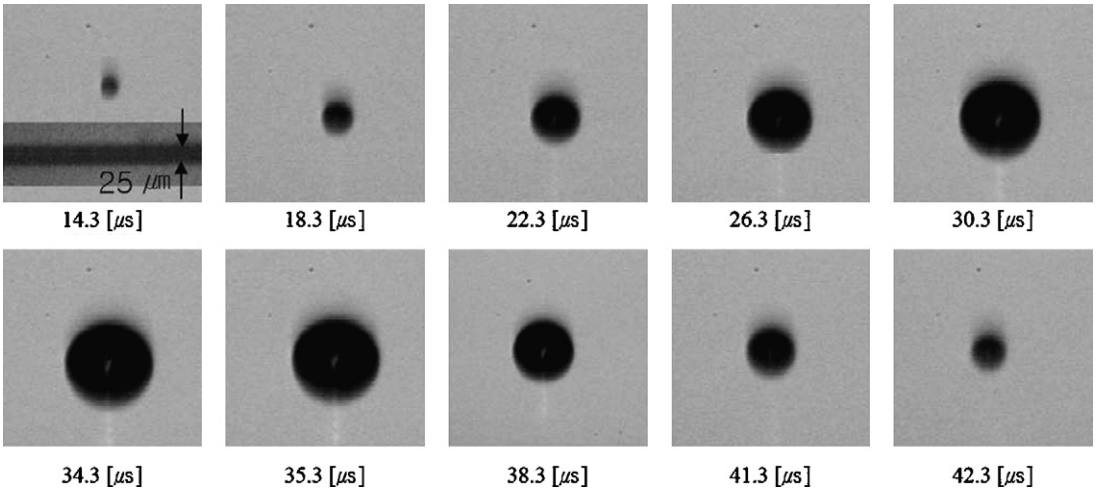

Fig. 8. Snapshot images of the oscillating bubble with SL shown in Fig. 2. A dark bar in the first frame is the image of gold wire of 25 μm diameter (from reference [21]).

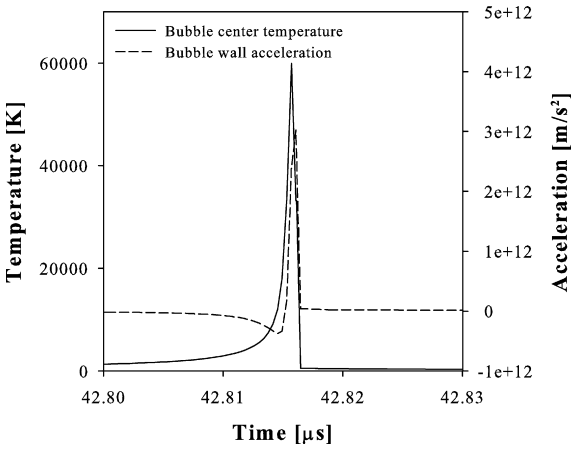

Fig. 9. Time-dependent center temperature and the bubble wall acceleration near the collapse point for the bubble shown in Fig. 7.

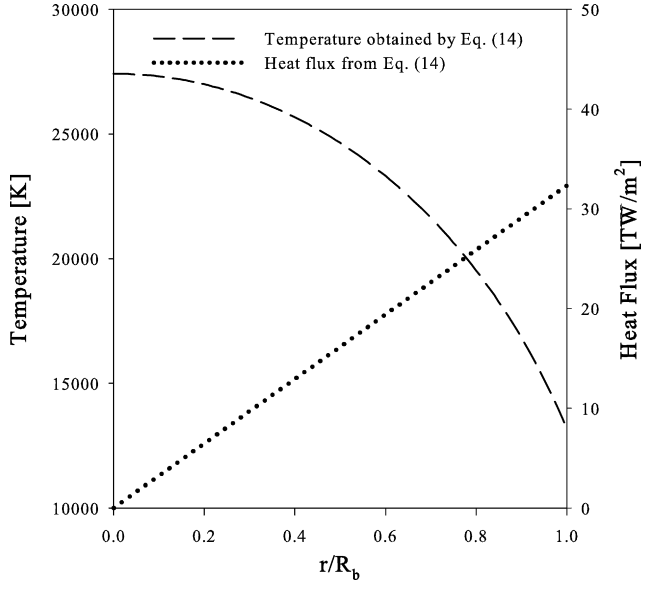

Fig. 10. Temperature distribution and heat flow rate per unit volume inside the bubble at the collapse point for the case shown in Fig. 8.

from Fig. 12b, the pressure value at the point where the temperature is 647 K, the critical temperature of water is much greater than the critical pressure of water, 218 atm, so that the supercritical state of water is developed above $T = 647$ K. Below 647 K, the pressure values are always greater than the saturation pressure corresponding to the temperature so that no evaporation takes place in the liquid layer. The estimated duration of supercritical state of water from Fig. 12a is about 400 ps. In fact, Hua et al. [53] noticed that high temperature and pressure exceeding the critical value of water at the interface during the bubble collapse and estimated the lifetime and spatial extent of the supercritical state by solving the transient conduction equation in the liquid layer. Much higher reaction rate of the hydrolysis of *p*-nitrophenyl acetate by several orders of magnitude in the presence of ultrasound was considered to be attributed to the existence of transient supercritical state of water during the bubble collapse [54]. The possibility of evaporation of liquid at the bubble wall is scarce because the temperature at the interface remains the same as

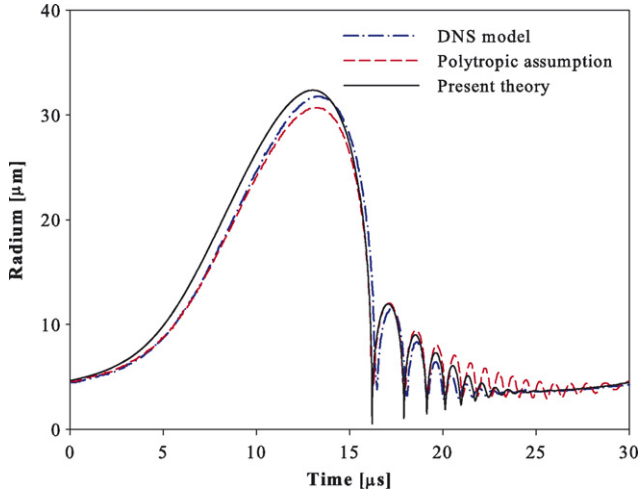

Fig. 11. Bubble radius–time curves by a direct numerical simulation, polytropic assumption and our analytical method for a 4.5 μm radius bubble driven at $P_A = 1.3$ atm and $f_d = 32.8$ kHz.

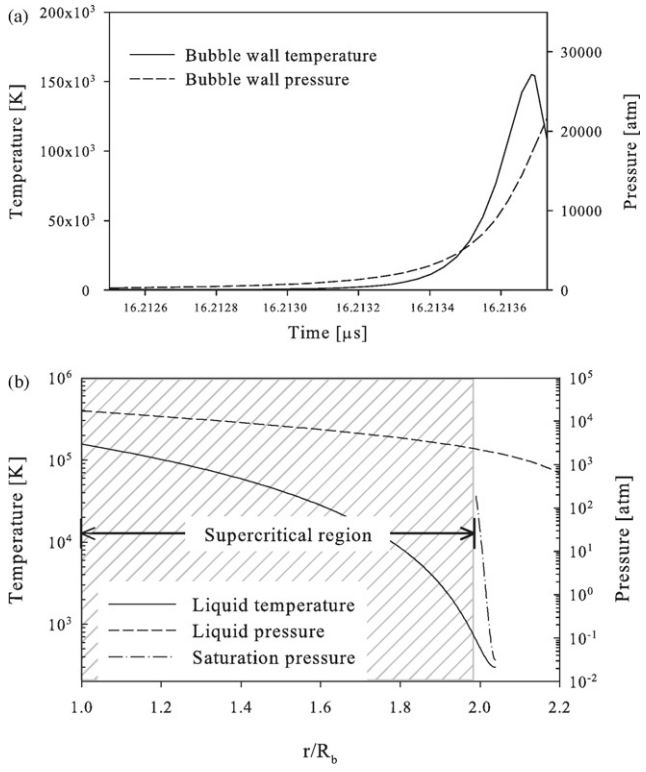

Fig. 12. (a) Time-dependent bubble wall temperature and pressure around the collapse point. (b) Calculated temperature and pressure distribution in the liquid layer adjacent to the bubble wall for the case shown in Fig. 11 at the collapse point.

the ambient temperature as shown in Fig. 2 except the collapse phase when the supercritical state of water is developed.

Finally, it is noted that the peak temperature and pressure at the collapse point turned out to be not affected by the mass transfer of gases through the bubble wall [55].

5. Conclusion

High temperature and pressure fields resulting from the collapse of microsize bubbles in liquids under ultrasound, which are responsible for the observed chemical and biological effects of ultrasound have been estimated by a set of solutions of the Navier–Stokes equations with consideration of heat transfer through the bubble wall. The calculated results of the peak temperature and pressure obtained by using our analytical model are in good agreement with the observed ones from a single sonoluminescing gas bubble which can be levitated in a cylindrical or spherical cell at the frequency range from 10 to 40 kHz of ultrasound. Our analytical model also produces correct radial motion of bubble, which is in good agreement with the result by direct numerical simulation, and the alternating pattern of bubble motion showing on/off sonoluminescence due to heat transfer across the interface in sulfuric acid solutions. In summary, our model presented in this study is an unique analytical one which can predict the behavior of the gas inside the evolving bubble. So, the analytical model used may be employed to the design of sonochemical reactors where the correct value of the parameters related to the cavitation intensity is required.

Acknowledgements

This work has been supported by the Seoul R&BD program (2006) and by a grant from Electric Power Research Institute (EPRI) in USA, under contract EP-P19394/C9578. One (Ki Young Kim) of authors has been also supported by the second stage of BK21 program.

References

[1] K.S. Suslick, Ultrasound: Its Chemical, Physical, and Biological Effects, VCH, New York, 1988.
[2] M.A. Margulis, Sonochemistry and Cavitation, Gordon and Breach, Amsterdam, 1995.
[3] K.S. Suslick, D.A. Hammerton, R.E. Cline, J. Am. Chem. Soc. 108 (1986) 5641–5642.
[4] A. Kotronarou, G. Mills, M.R. Hoffmann, J. Phys. Chem. 95 (1991) 3630–3638.
[5] E. Psillakis, G. Goula, N. Kalogerakis, D. Mantzavinos, J. Hazard. Mater. 108 (2004) 95–102.
[6] K.S. Suslick, M.M. Fang, T. Hyeon, M.M. Midleleni, in: L.A. Crum, et al. (Eds.), Sonochemistry and Sonoluminescence, Kluwer Publishers, Netherlands, 1999.
[7] S.S. Manoharan, M.L. Rao, in: H.S. Nalwa (Ed.), Encyclopedia of Nanoscience and Nanotechnology, vol. 10, American Scientific Publishers, 2004, pp. 67–82.
[8] K. Byun, H. Kwak, J. Photochem. Photobiol. A: Chem. 175 (2005) 45–50.
[9] S.S. Lee, K.W. Seo, S.H. Yoon, I. Shim, K. Byun, H. Kwak, Bull. Korean Chem. Soc. 26 (2005) 1579–1581.
[10] R. Feng, Y. Zhao, C. Zhu, T.J. Mason, Ultrason. Sonochem. 9 (2002) 231–236.
[11] P.R. Gogate, P.A. Tatake, P.M. Kanthale, A.B. Pandit, AIChE J. 48 (2002) 1542–1560.
[12] P.R. Gogate, A.B. Pandit, Ultrason. Sonochem. 11 (2004) 105–117.
[13] K.Y. Kim, K. Byun, H. Kwak, J. Phys. Soc. Jpn. 75 (2006) 114705.
[14] S.D. Hopkins, S.J. Putterman, B.A. Kappus, K.S. Suslick, C.G. Camara, Phys. Rev. Lett. 95 (2005) 254301.
[15] D.J. Flannigan, S.D. Hopkins, C.G. Camara, S.J. Putterman, K.S. Suslick, Phys. Rev. Lett. 96 (2006) 204301.
[16] A. Prosperetti, L.A. Crum, K.W. Commander, J. Acoust. Soc. Am. 83 (1988) 502–514.
[17] H. Kwak, S. Oh, C. Park, Int. J. Heat Mass Transfer 38 (1995) 1709–1718.
[18] H. Kwak, H. Yang, J. Phys. Soc. Jpn. 64 (1995) 1980–1992.
[19] N.A. Tsochatzidis, P. Guiraud, A.M. Wilhelm, H. Delmas, Chem. Eng. Sci. 56 (2001) 1831–1840.
[20] H. Kwak, J. Lee, S.W. Karng, J. Phys. Soc. Jpn. 70 (2001) 2909–2917.
[21] J. Jeon, J. Lee, H. Kwak, J. Phys. Soc. Jpn. 72 (2003) 509–515.
[22] S.W. Karng, H. Kwak, Jpn. J. Appl. Phys. 45 (2006) 317–322.
[23] D.F. Gaitan, L.A. Crum, C.C. Church, R.A. Roy, J. Acoust. Soc. Am. 91 (1992) 3166–3183.
[24] B.P. Barber, R.A. Hiller, R. Löfstedt, S.J. Putterman, K.R. Weninger, Phys. Rep. 281 (1997) 65–143.
[25] R.F. Young, Sonoluminescence, CRC Press, 2005.
[26] R.L. Panton, Incompressible Flow, 2nd ed., John Wiley & Sons Inc., New York, 1996.
[27] H. Kwak, J.H. Na, J. Phys. Soc. Jpn. 66 (1997) 3074–3083.
[28] J. Jun, H. Kwak, Int. J. Mod. Phys. D 9 (2000) 35–42.
[29] H. Lin, B.D. Storey, A.J. Szeri, J. Fluid Mech. 452 (2002) 145–162.
[30] H. Kwak, J.H. Na, Phys. Rev. Lett. 77 (1996) 4454–4457.
[31] C.C. Wu, P.H. Robert, Phys. Rev. Lett. 70 (1993) 3424–3427.
[32] W.C. Moss, D.B. Clarke, J.W. White, D.A. Young, Phys. Fluids 6 (1994) 2979–2985.
[33] K. Yasui, J. Acoust. Soc. Am. 98 (1995) 2772–2782.
[34] J. Jeon, I. Yang, J. Na, H. Kwak, J. Phys. Soc. Jpn. 69 (2000) 112–119.
[35] J. Kestin, K. Knierim, E.A. Mason, B. Najafi, S.T. Ro, M. Waldman, J. Phys. Chem. Ref. Data 13 (1984) 229–303.

[36] K. Byun, H. Kwak, S.W. Karng, Jpn. J. Appl. Phys. 43 (2004) 6364–6370.
[37] R.C. Davidson, Methods in Nonlinear Plasma Theory, Academic Press, New York, 1972.
[38] M.I. Boulos, P. Fauchais, E. Pfender, Thermal Plasma, vol. 1, Plenum Press, New York, 1994.
[39] J.B. Keller, M. Miksis, J. Acoust. Soc. Am. 68 (1980) 628–633.
[40] T. Theofanous, L. Biasi, H.S. Isbin, H. Fauske, Chem. Eng. Sci. 24 (1969) 885–897.
[41] L.E. Scriven, Chem. Eng. Sci. 10 (1959) 1–13.
[42] J. Na, G. Byun, H. Kwak, J. Korean Phys. Soc. 42 (2003) 143–152.
[43] V. Kamath, A. Prosperetti, J. Acoust. Soc. Am. 85 (1989) 1538–1548.
[44] S. Hilgenfeldt, S. Grossman, D. Lohse, Phys. Fluids 11 (1999) 1318–1330.
[45] U. Parlitz, V. Englisch, C. Scheffczyk, W. Lauterborn, J. Acoust. Soc. Am. 88 (1990) 1061–1077.
[46] A. Prosperetti, J. Acoust. Soc. Am. 61 (1977) 17–27.
[47] A. Prosperetti, Y. Hao, Philos. Trans. R. Soc. London A 357 (1999) 203–223.
[48] R. Löfstedt, B.P. Barber, S.J. Putterman, Phys. Fluids A 5 (1993) 2911–2928.
[49] H. Kwak, S.W. Karng, Y.P. Lee, J. Korean Phys. Soc. 46 (2005) 951–962.
[50] A. Troia, D.M. Ripa, R. Spagnolo, This Paper was Presented at World Congress of Ultrasonics 2003, Paris, Ultrason. Sonochem. 13 (2006) 278–282.
[51] K.R. Weninger, B.P. Barber, S.J. Putterman, Phys. Rev. Lett. 78 (1997) 1799–1802.
[52] B.D. Storey, Phys. Rev. E 64 (2001) 017301.
[53] I. Hua, R.H. Hochemer, M.R. Hoffmann, J. Phys. Chem. 99 (1995) 2335–2342.
[54] H. Hung, M.R. Hoffmann, J. Phys. Chem. A 103 (1999) 2734–2739.
[55] K.Y. Kim, H. Kwak, Predictions of bubble behavior in sulfuric acid solutions by a set of solutions Navier–Stokes equations, submitted for publication.